

# Pressure-induced densification of vitreous silica: insight from elastic properties

Coralie Weigel, Marouane Mebarki, Sébastien Clément, René Vacher, Marie Foret, and Benoit Rufflé\*  
*Laboratoire Charles Coulomb (L2C), University of Montpellier, CNRS, Montpellier, France.*

(Dated: May 13, 2022)

*In situ* high-pressure Brillouin light scattering experiments along loading-unloading paths are used to investigate the compressibility of vitreous silica. An accurate equation of state is obtained below 9 GPa using sound velocities corrected for dispersion. Conversely, huge inelastic effects are observed in the range 10–60 GPa, unveiling the reversible transformation from the fourfold-coordinated structure to the sixfold one. We find that the associated density changes fully correlate with the average Si coordination number. Decompression curves from above 20 GPa reveal abrupt backward coordination changes around 10–15 GPa and significant hysteresis. Further, contrary to common wisdom, the residual densification of recovered silica samples can be figured out from the pressure cycles.

Changes in the structure of network-forming glasses occur in response to applied pressure. Moreover, different amorphous states with distinct short- and/or intermediate-range orders as well as contrasting physical properties can be produced following separate thermomechanical paths. Even if these phenomena, termed *polyamorphism*, have been extensively studied during the last decades, their complete understanding still remain an ongoing challenge. It relates to the difficulty in carrying out conclusive experiments at high pressure. Beyond physics of the amorphous state, a comprehensive knowledge of polyamorphism has significance for the development of new functional glassy materials, particularly if novel high-pressure forms are recoverable to ambient conditions [1, 2].

Vitreous silica ( $v\text{-SiO}_2$ ) is the archetypal tetrahedral network-forming glass whose behavior under pressure is of long-standing interest due to its primary importance as the analog material of silicates in geophysics [3, 4].  $\text{SiO}_2$  glass presents remarkable properties when submitted to high pressure. For example, its compressibility  $\chi$  exhibits a maximum at about 2 GPa [5–7] accompanied by a concomitant sharp maximum in the internal friction [8–10]. Moreover, silica glass undergoes a change from an elastic behavior to a plastic one around 8–10 GPa at room temperature [11]. When compressed above 10 GPa, the recovered glasses exhibit residual densification up to  $\sim 20\%$  for a maximum pressure of  $\sim 25$  GPa [12]. *In situ* experiments at higher  $P$  show that the density of the squeezed silica glass further increases gradually and becomes comparable to that of stishovite, the sixfold coordinated crystalline polymorph, above 50 GPa [13]. The basic mechanisms of the  $\text{SiO}_2$  network collapse upon compression have been early identified as the reduction of the Si–O–Si bond angle between  $\text{SiO}_4$  tetrahedra below 10 GPa, and the progressive change in the Si coordination number from four to six at higher  $P$ , the latter being not quenchable at ambient  $P$  [12, 14–23].

Beyond structural studies, investigations of the thermodynamical and relaxational properties have proven to be enlightening. For instance, sound velocity measurements have revealed the anomalous negative pressure

derivatives of elastic moduli at low  $P$  [6]. They have also provided an equation of state (EoS) – density *vs* pressure – for  $v\text{-SiO}_2$  in the elastic domain [17, 24–26]. The stiffening of the elastic moduli, associated with permanent densification of the recovered glasses at ambient  $P$ , has also been evidenced many times [27–29]. Accurate volumetric experiments at pressures below 9 GPa have revealed several features of polyamorphism among which logarithmic kinetics and significant inelastic effects are the more salient ones [30–32]. However, most of the studies reported so far involve compression only. Although it is admitted that the high- $P$  octahedral structure of  $v\text{-SiO}_2$  reverts back to the tetrahedral one at ambient  $P$ , little is known about the rate of this transformation and its relation with other properties like density or elastic properties. The same is true for the permanent densification process. In this Letter, we re-investigate the variations of sound velocities in  $v\text{-SiO}_2$  using pressure cycles and *in situ* Brillouin light scattering experiments of unprecedented quality. Combined with density data we provide a series of quantitative results related both to the reversible and the irreversible transformations along the loading-unloading paths.

High pressures were generated using Chervin-type diamond anvil cells (DAC) with culetts of 400  $\mu\text{m}$  diameter. Samples of about  $50 \times 50 \mu\text{m}^2$  were made from a 15  $\mu\text{m}$  thick polished plate of Tetrasil SE fused silica ( $[\text{OH}] \simeq 100$  ppm). They were each loaded in a chamber of 150  $\mu\text{m}$  diameter drilled in rhenium gasket together with ruby-spheres to measure the pressure [33]. The accuracy on pressure measurements was 0.1 GPa and the pressure-transmitting medium was argon fluid to ensure an hydrostatic stress up to the highest pressures. *In situ* high pressure Brillouin scattering experiments were performed using a standard triple-pass tandem interferometer [34] and a single line diode-pumped solid-state laser operating at  $\lambda_0 = 532$  nm. All the measurements were obtained at room temperature in the symmetric platelet geometry with a scattering angle of  $50^\circ$  [25]. The aperture angle was limited using a curved slit matching the spurious geometrical broadening of the Brillouin lines to the resolution of the spectrometer [35]. From the Brill-

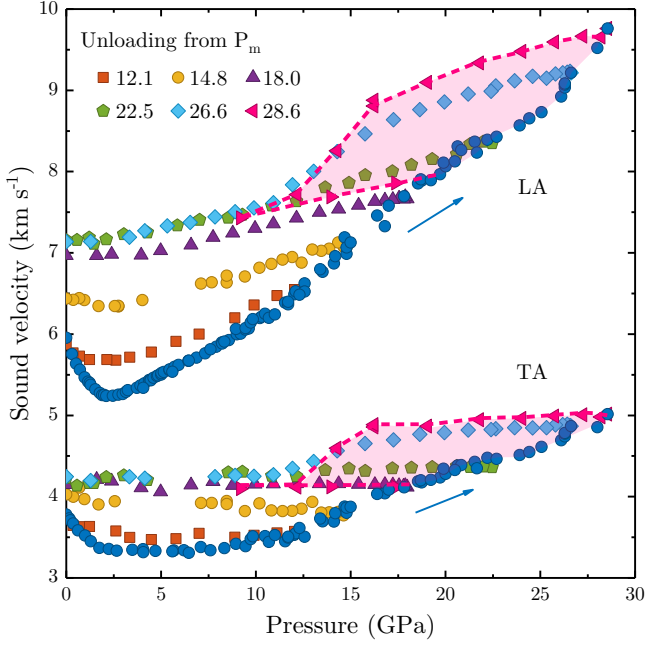


FIG. 1. Longitudinal (LA) and transverse (TA) sound velocities in  $v$ -SiO<sub>2</sub> upon compression (●) and during decompression from various maximum pressures  $P_m$ . The pink dashed line is a guide for the eye.

loun frequency shifts, the longitudinal and transverse acoustic velocities,  $v_{LA}$  and  $v_{TA}$  respectively, are obtained. These are related to the bulk modulus  $K$  and to the shear modulus  $G$ ,

$$v_{LA} = \sqrt{\frac{K + \frac{4}{3}G}{\rho}}, \quad v_{TA} = \sqrt{\frac{G}{\rho}}, \quad (1)$$

where  $\rho$  is the density.

Compression-decompression cycles reaching various maximum pressures  $P_m$  extending up to nearly 30 GPa have been carried out. As expected, the results found upon compression for both LA and TA velocities, shown as blue circles in Fig. 1, superimpose on a single curve for all cycles. For  $P_m \lesssim 10$  GPa, the values of the sound velocities upon decompression also match the ones on compression within the accuracy of the measurements. The other symbols in Fig. 1 show the results acquired for decompression paths from higher  $P_m$  ranging from 12.1 to 28.6 GPa. Upon decompression, the velocities are larger than those obtained in the compression part of the cycles, indicating an irreversible behavior after complete release of  $P$ , but also revealing unsuspected hysteresis phenomena at high  $P$  (pink shaded area in Fig. 1). These two points will be discussed later on.

We start our analysis by focusing on the low  $P$  part of the compression. Fig. 2 shows the density increase of  $v$ -SiO<sub>2</sub> as a function of the applied pressure for  $P \lesssim 9$  GPa. The squares are from volumetric measurements using an

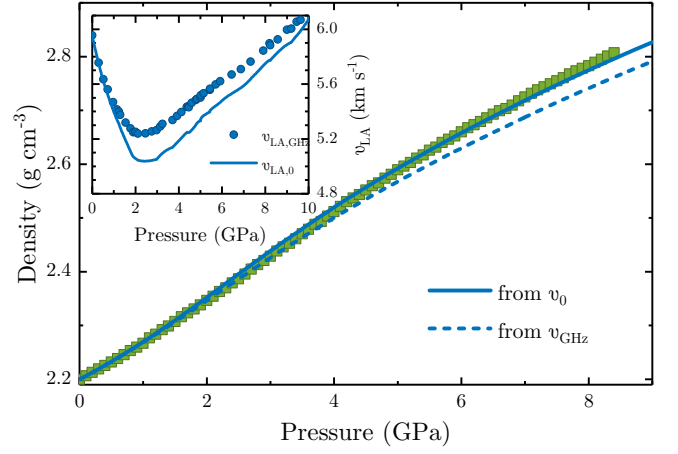


FIG. 2. Density of  $v$ -SiO<sub>2</sub> from volumetric experiments (■ [30]), compared to values computed from Eq. 2 using the hypersonic velocities, as measured ( $v_{GHz}$  dashed line) or corrected from dispersion effects ( $v_0$  solid line). Inset: LA velocities  $v_{LA,GHz}(P)$  (●) and associated relaxed velocities  $v_{LA,0}(P)$ .

accurate strain-gauge technique [30], thus referring to the static compressibility  $\chi_0$ . For an isotropic and elastic material, the density can also be computed from the sound velocities [17, 24]:

$$\rho(P) = \rho_0 + \int_0^P \gamma v_K^{-2} dP, \quad (2)$$

where  $v_K^2 = v_{LA}^2 - \frac{4}{3}v_{TA}^2 = K/\rho = 1/\rho\chi$  and  $\gamma$  is the heat capacity ratio, very close to 1 in glasses and especially in  $v$ -SiO<sub>2</sub>. However, in this case, viscoelastic effects must be taken into account. The dashed line in Fig. 2 is the  $\rho(P)$  curve calculated using the velocities acquired upon compression. The latter is slightly lower than the static values. This is actually explained by the frequency dependence of sound velocities caused by internal friction. Two dissipative processes dominate in glasses (See S-I in Supplemental Material): the interaction with relaxing structural entities called *defects* [36, 37] and the anharmonic interactions with thermal vibrations [38]. Accordingly, sound velocities should vary between a low-frequency (relaxed) value  $v_0$  and a high-frequency (unrelaxed) one  $v_\infty$ . A quantitative description of velocity dispersion exists for  $v$ -SiO<sub>2</sub> [39] which has been extended to high pressures [9], resulting in the  $v_0(P)$  curve for LA modes, significantly lower than velocities at GHz frequencies (inset in Fig. 2 and Fig. S1 in Supplemental Material). Using the relaxed velocities  $v_{LA,0}(P)$  and  $v_{TA,0}(P)$  [40], a new  $\rho(P)$  curve is determined from Eq. 2 which is plotted as a solid line in Fig. 2. These new  $\rho(P)$  variations are appreciably larger than those deduced from uncorrected velocities, and stand very close to the static values. This result highlights the need to take into account the viscoelastic character of the medium to obtain an accurate EoS.

In contrast, at higher  $P$  the corrected  $v_K$  values do not

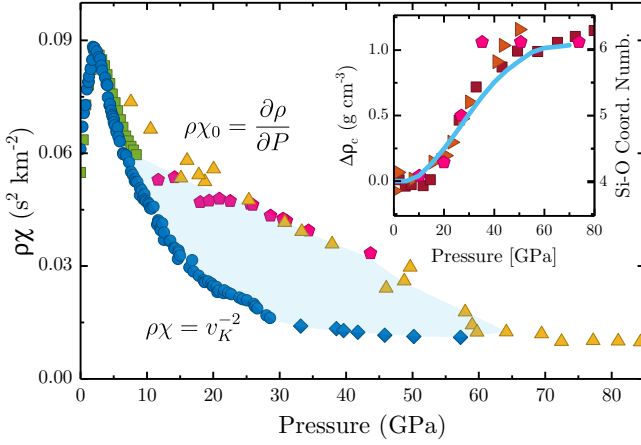


FIG. 3. Static quantity  $\rho\chi_0 = \frac{\partial\rho}{\partial P}$  from density data (■ [30], ◆ [13], ▲ [41]) and  $\rho\chi = v_K^{-2}$  from BLS (●, ◆ [17]), upon compression. Inset: Density increase from Eq.3 (solid line) compared to the mean Si–O coordination number (▶ [19], ◆ [20] and ■ [23]) on the same relative scale.

give the right EoS and thus the static compressibility  $\chi_0$  as shown in Fig. 3, where the pressure dependence of the elastic quantity  $\rho\chi = v_K^{-2}$  upon compression (blue circles) is plotted. Our data are completed by those of Zha *et al.* [17] at the highest  $P$  (blue lozenges). This quantity is relevant since it gives the density variation  $\delta\rho$  associated with a pressure variation  $\delta P$ , see Eq. 2. The  $\rho\chi$  values can be compared to the static ones,  $\rho\chi_0 = \partial\rho/\partial P$ , calculated using densities from literature [13, 30, 41], and also shown in Fig. 3 (See also S-II and Fig. S3 in Supplemental Material for a similar graph of the bulk moduli  $K$  and  $K_0$ ). Following Fig. 2,  $\rho\chi$  and  $\rho\chi_0$  superimpose in the elastic domain below  $\sim 9$  GPa. Above,  $\rho\chi$  decreases much more rapidly than  $\rho\chi_0$ , their ratio reaching a factor 3 around 30 GPa. At  $P \simeq 60$  GPa the two curves merge again. The large difference between the two compressibilities is the well-known fingerprint for either intense relaxation processes or significant structural transformations. The onset of these inelastic effects was reported previously for  $v$ -SiO<sub>2</sub> by El'kin *et al.* [30] and for other structural glasses by Brazhkin *et al.* [31, 32], but to our knowledge, this is the first observation of the complete process between the two regimes for which the glass mostly responds elastically, *i.e.* when  $\chi \simeq \chi_0$ . The compaction  $\Delta\rho_c$  associated with the difference between the two  $\rho\chi$  curves simply relates to very slow processes which are frozen in at the high BLS frequencies. Accordingly,  $\chi$  is an unrelaxed value for these processes whereas  $\chi_0$  is a quasi-static one – not exactly the static one – because these transformations obey slow logarithmic kinetics with timescales exceeding hours [30, 31]. The compaction  $\Delta\rho_c$  can be estimated from the blue area in Fig. 3:

$$\Delta\rho_c(P) = \int_0^P (\rho\chi_0 - \rho\chi) dP. \quad (3)$$

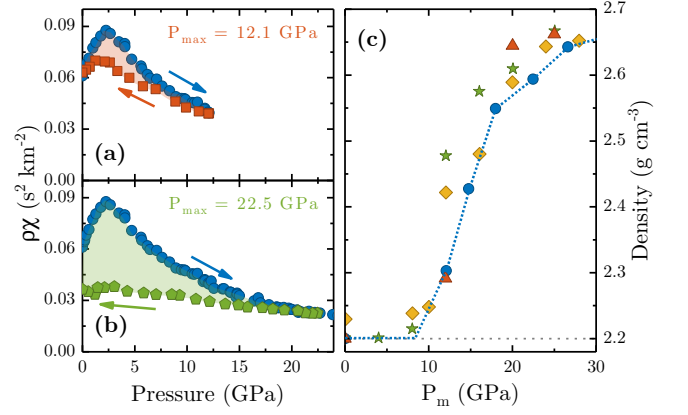


FIG. 4. (a) and (b)  $v_K^{-2}$  along a compression-decompression cycle for two different  $P_m$  values. The shaded area represents the residual densification  $\Delta\rho_r = \rho_f - \rho_0$ . (c) Final density  $\rho_f$  vs  $P_m$  (from Eq. 4 ●, ▲ [42], ★ [43], ◆ [44]). The dotted line is a guide for the eye.

The latter quantity is reported in the inset in Fig. 3 as a solid line. The compaction gently starts below 10 GPa to eventually end up around 60 GPa, having its maximum rate around 30 GPa. The mean Si–O coordination number from recent experiments [19, 20, 23] is also plotted using the same relative scale, resulting in a remarkable superposition of both quantities. They almost increase at the same rate, suggesting that the calculated compaction  $\Delta\rho_c$  originates from the progressive transformation from the fourfold-coordinated structure to the sixfold one. An increase in density of about  $1 \text{ g cm}^{-3}$  is obtained for the complete process. Fig. 3 thus illustrates how density and sound velocity measurements unveil the pressure window of such structural transformations.

We now turn to the unloading part of the cycles for  $P_m \gtrsim 10$  GPa. Comparing the decompression curve from  $P_m = 28.6$  GPa (pink left triangles in Fig. 1) to the one from  $P_m = 22.5$  GPa (green pentagons), we first remark that significantly larger velocities are found at high  $P$  for the former, while both curves coincide on the low- $P$  side. Re-increasing the pressure from 9 GPa (pink right triangles), we observe further that the velocities behave differently from the decompression curve and merge eventually with the initial compression one at  $\sim 19$  GPa. This suggests an hysteresis phenomenon, illustrated as a pink shaded area. The latter is likely due to the fivefold- and sixfold-coordinated Si atoms remaining stable during decompression, while the return to the fourfold ones occurs between 10–15 GPa and more abruptly than the progressive direct transformation upon compression. There are indeed some converging indications of rapid changes upon decompression from diffraction experiments [45] as well as from *ab initio* molecular dynamics simulations [46]. Further, similar behaviors were also reported for the trigonally coordinated network former  $v$ -B<sub>2</sub>O<sub>3</sub> [31, 47–49].

It was proposed that changes in the B–O coordination number were gradual upon compression but abrupt at the time of decompression [47, 48], an interpretation which has however been questioned [50].

Finally, we address the issue of the permanent densification. As shown in Fig. 1, the final sound velocity after a complete pressure release is generally higher than that of the pristine sample, reflecting an irreversible behavior. This final value increases strongly when  $P_m$  goes from 12.1 to 18 GPa and tends to saturate above. As already mentioned, the changes in the mean Si–O coordination number cannot be quenched to ambient pressure at room temperature in  $v$ -SiO<sub>2</sub> [12, 15, 17, 22]. The associated compaction  $\Delta\rho_c$  acquired upon compression is thus expected to vanish along the unloading path. According to Eq. 2, the open loop in the sound velocities should then reflect the final residual densification  $\Delta\rho_r$ , which for a complete cycle up to  $P_m$ , reads:

$$\Delta\rho_r(P_m) = \int_0^{P_m} (v_{k,ul}^{-2} - v_{k,l}^{-2}) dP, \quad (4)$$

where  $v_{k,l}$  and  $v_{k,ul}$  are the velocities along loading and unloading path, respectively. Figs. 4a and 4b illustrate the  $P$  variations of  $v_k^{-2}$  along a cycle for two different  $P_m$ . The shaded area, which reflects the residual densification, increases with increasing  $P_m$ . The final densities  $\rho_f = \rho_0 + \Delta\rho_r$  of the recovered samples are shown in Fig. 4(c) as a function of  $P_m$  (blue circles). As expected,  $\rho_f$  starts to increase for  $P_m \gtrsim 10$  GPa until about 20 GPa beyond which it tends to saturate at  $\rho \simeq 2.65 \text{ g cm}^{-3}$ . Our results compare fairly well to other estimates based on numerical simulations [43, 44] also plotted in Fig. 4(c). While showing the same general trend, they exhibit slightly larger  $\rho_f$  in the initial stages of the densification process. Some other numerical results show qualitatively similar results, albeit with a larger densification rate [10]. To our knowledge, there exists only one set of experimental data for  $\rho_f$  vs  $P_m$  as a result of hydrostatic compression at room temperature (red triangles [42]) allowing a comparison with our results at 12 GPa and above 20 GPa. The latter densities also agree with our outputs. If the  $\Delta\rho_r$  had been calculated from the BLS velocities without being corrected for the dynamical dissipative effects, they would have been underestimated by about 10% (See S-I and Fig. S2 in Supplemental Material). We also note that the hysteresis at high  $P$ , ascribed to changes in the coordination number, affects the estimate of the residual densification for the highest  $P_m$ , however marginally due to the very low compressibility of the compacted network (See S-III and Fig. S4 in Supplemental Material). It is then remarkable that, even if the pressure variation of the density cannot be obtained from the sound velocities using Eq. 2 due to the inelastic effects, the residual densification can be completely figured out from them. This indicates that the process leading to the permanent densification, as-

sociated with changes in the network topology, is an almost instantaneous phenomenon at the Brillouin frequency scale, as is the elastic response of the medium. Conversely, the fourfold to sixfold structural transformation is almost frozen in at the Brillouin frequency scale. Hence, the sound velocities extracted from the BLS experiments are relaxed velocities for the former process while they are mainly unrelaxed ones for the latter. The large difference in time-scale of the two processes allows to study them separately even if their pressure windows overlap.

Summarizing, we show that the large difference between the static compressibility and that extracted from BLS experiments can be used to monitor the pressure window where slow structural rearrangements occur in vitreous silica. The associated compaction and its rate are quantified and successfully compared to structural informations, the compaction being closely related to the Si–O average coordination number. Moreover, this transformation displays a significant hysteresis. Out of this pressure window, vitreous silica behaves almost elastically and the equation of state can be recovered from the sound velocities corrected from the dispersion effects, significant at low pressure. Finally, we find out that the large open-loop hysteresis observed in the sound velocity data along the loading-unloading path does account for the residual densification of the recovered silica samples, at odds with the common belief.

More generally, this work also shows that complete pressure cycles certainly deserve more attention and that precise density *and* sound velocity measurements, when combined, give fundamental insights into pressure-induced transformations in glasses. That would be definitely interesting to address the case of  $v$ -B<sub>2</sub>O<sub>3</sub> or  $v$ -GeO<sub>2</sub> for example. For the latter, there are indications that polyamorphism with coordination numbers higher than six occurs above 30 GPa [51, 52], which would justify similar work. Concerning  $v$ -B<sub>2</sub>O<sub>3</sub>, such approach should help in solving the controversy existing about the rapid changes in the structure and the elastic properties upon decompression.

This work was supported by the French National Research Agency programs MECASIL ANR-12-BS04-0004-03 and PIPOG ANR-17-CE30-0009.

---

\* Corresponding author: benoit.ruffle@umontpellier.fr

- [1] P. McMillan, Nat. Mater. **1**, 19 (2002).
- [2] V. Brazhkin, High Pressure Res. **27**, 333 (2007).
- [3] C. Sanloup, J. W. E. Drewitt, Z. Konopkova, P. Dalladay-Simpson, D. M. Morton, N. Rai, W. van Westrenen, and W. Morgenroth, Nature **503**, 104 (2013).
- [4] M. Millot, N. Dubrovinskaia, A. Černok, S. Blaha, L. Dubrovinsky, D. G. Braun, P. M. Celliers, G. W. Collins, J. H. Eggert, and R. Jeanloz, Science **347**, 418

- (2015).
- [5] P. Bridgman, Am. J. Sci. **237**, 7 (1939).
  - [6] K. Kondo, S. Lio, and A. Sawaoka, J. Appl. Phys. **52**, 2826 (1981).
  - [7] L. Huang and J. Kieffer, Phys. Rev. B **69**, 224203 (2004).
  - [8] U. Bartell and S. Hunklinger, J. Phys. Colloques **43**, 489 (1982).
  - [9] S. Ayrihac, B. Rufflé, M. Foret, H. Tran, S. Clément, R. Vialla, R. Vacher, J. C. Chervin, P. Munsch, and A. Polian, Phys. Rev. B **84**, 024201 (2011).
  - [10] B. Mantisi, A. Tanguy, G. Kermouche, and E. Barthel, Eur. Phys. J. B **85**, 304 (2012).
  - [11] P. W. Bridgman and I. Simon, J. Appl. Phys. **24**, 405 (1953).
  - [12] S. Susman, K. J. Volin, D. L. Price, M. Grimsditch, J. P. Rino, R. K. Kalia, P. Vashishta, G. Gwanmesia, Y. Wang, and R. C. Liebermann, Phys. Rev. B **43**, 1194 (1991).
  - [13] T. Sato and N. Funamori, Phys. Rev. Lett. **101**, 255502 (2008).
  - [14] R. J. Hemley, H. K. Mao, P. M. Bell, and B. O. Mysen, Phys. Rev. Lett. **57**, 747 (1986).
  - [15] Q. Williams and R. Jeanloz, Science **239**, 902 (1988).
  - [16] C. Meade, R. J. Hemley, and H. K. Mao, Phys. Rev. Lett. **69**, 1387 (1992).
  - [17] C.-s. Zha, R. J. Hemley, H.-k. Mao, T. S. Duffy, and C. Meade, Phys. Rev. B **50**, 13105 (1994).
  - [18] V. V. Brazhkin, Phys. Rev. Lett. **102**, 209603 (2009).
  - [19] C. J. Benmore, E. Soignard, S. A. Amin, M. Guthrie, S. D. Shastri, P. L. Lee, and J. L. Yarger, Phys. Rev. B **81**, 054105 (2010).
  - [20] T. Sato and N. Funamori, Phys. Rev. B **82**, 184102 (2010).
  - [21] A. Zeidler, K. Wezka, R. F. Rowlands, D. A. J. Whittaker, P. S. Salmon, A. Polidori, J. W. E. Drewitt, S. Klotz, H. E. Fischer, M. C. Wilding, C. L. Bull, M. G. Tucker, and M. Wilson, Phys. Rev. Lett. **113**, 135501 (2014).
  - [22] N. M. Trease, T. M. Clark, P. J. Grandinetti, J. F. Stebbins, and S. Sen, J. Chem. Phys. **146**, 184505 (2017).
  - [23] C. Prescher, V. B. Prakapenka, J. Stefanski, S. Jahn, L. B. Skinner, and Y. Wang, Proc. Natl. Acad. Sci. **114**, 10041 (2017).
  - [24] J. Schroeder, T. G. Bilodeau, and X.-S. Zhao, High Pressure Res. **4**, 531 (1990).
  - [25] C. Weigel, A. Polian, M. Kint, B. Rufflé, M. Foret, and R. Vacher, Phys. Rev. Lett. **109**, 245504 (2012).
  - [26] B. Coasne, C. Weigel, A. Polian, M. Kint, J. Rouquette, J. Haines, M. Foret, R. Vacher, and B. Ruffl, J. Phys. Chem. B **118**, 14519 (2014).
  - [27] M. Grimsditch, Phys. Rev. Lett. **52**, 2379 (1984).
  - [28] A. Polian and M. Grimsditch, Phys. Rev. B **41**, 6086 (1990).
  - [29] T. Rouxel, H. Ji, J. P. Guin, F. Augereau, and B. Rufflé, J. Appl. Phys. **107**, 094903 (2010).
  - [30] F. El'kin, V. Brazhkin, L. Khvostantsev, O. Tsiok, and A. Lyapin, JETP Lett. **75**, 342 (2002).
  - [31] V. V. Brazhkin, Y. Katayama, K. Trachenko, O. B. Tsiok, A. G. Lyapin, E. Artacho, M. Dove, G. Ferlat, Y. Inamura, and H. Saitoh, Phys. Rev. Lett. **101**, 035702 (2008).
  - [32] V. V. Brazhkin, E. Bychkov, and O. B. Tsiok, J. Phys. Chem. B **120**, 358 (2016).
  - [33] J.-C. Chervin, B. Canny, and M. Mancinelli, High Pressure Res. **21**, 305 (2001).
  - [34] S. M. Lindsay, M. W. Anderson, and J. R. Sandercock, Rev. Sci. Instrum. **52**, 1478 (1981).
  - [35] R. Vacher, S. Ayrihac, M. Foret, B. Rufflé, and E. Courtens, Phys. Rev. B **74**, 012203 (2006).
  - [36] O. L. Anderson and H. E. Bömmel, J. Am. Ceram. Soc. **38**, 125.
  - [37] J. Jäckle, L. Piché, W. Arnold, and S. Hunklinger, J. Non-Cryst. Solids **20**, 365 (1976).
  - [38] H. J. Maris, in *Physical Acoustics*, Vol. VIII, edited by W. Mason and R. Thurston (Academic Press, New York, NY, 1971) p. 279.
  - [39] R. Vacher, E. Courtens, and M. Foret, Phys. Rev. B **72**, 214205 (2005).
  - [40] B. Rufflé, S. Ayrihac, E. Courtens, R. Vacher, M. Foret, A. Wischnewski, and U. Buchenau, Phys. Rev. Lett. **104**, 067402 (2010).
  - [41] S. Petitgirard, W. J. Malfait, B. Journaux, I. E. Collings, E. S. Jennings, I. Blanchard, I. Kantor, A. Kurnosov, M. Cotte, T. Dane, M. Burghammer, and D. C. Rubie, Phys. Rev. Lett. **119**, 215701 (2017).
  - [42] T. Rouxel, H. Ji, T. Hammouda, and A. Moréac, Phys. Rev. Lett. **100**, 225501 (2008).
  - [43] S. Sundararaman, L. Huang, S. Ispas, and W. Kob, J. Chem. Phys. **148**, 194504 (2018).
  - [44] Y. Liang, C. R. Miranda, and S. Scandolo, Phys. Rev. B **75**, 024205 (2007).
  - [45] T. Sato, N. Funamori, D. Wakabayashi, K. Nishida, and T. Kikegawa, Phys. Rev. B **98**, 144111 (2018).
  - [46] E. Ryuo, D. Wakabayashi, A. Koura, and F. Shimojo, Phys. Rev. B **96**, 054206 (2017).
  - [47] J. Nicholas, S. Sinogeikin, J. Kieffer, and J. Bass, Phys. Rev. Lett. **92**, 215701 (2004).
  - [48] L. Huang, J. Nicholas, J. Kieffer, and J. Bass, J. Phys.-Cond. Matter **20**, 075107 (2008).
  - [49] A. Zeidler, K. Wezka, D. A. J. Whittaker, P. S. Salmon, A. Baroni, S. Klotz, H. E. Fischer, M. C. Wilding, C. L. Bull, M. G. Tucker, M. Salanne, G. Ferlat, and M. Micoulaut, Phys. Rev. B **90**, 024206 (2014).
  - [50] V. V. Brazhkin, O. B. Tsiok, and Y. Katayama, JETP Letters **89**, 244 (2009).
  - [51] V. V. Brazhkin, A. G. Lyapin, and K. Trachenko, Phys. Rev. B **83**, 132103 (2011).
  - [52] Y. Kono, C. Kenney-Benson, D. Ikuta, Y. Shibazaki, Y. Wang, and G. Shen, Proc. Natl. Acad. Sci. **113**, 3436 (2016).